JACS
JOURNAL OF THE AMERICAN CHEMICAL SOCIETY
Cite This: J. Am. Chem. Soc. 2019, 141, 753−757
Communication
pubs.acs.org/JACS

Tip-Enhanced Raman Imaging of Single-Stranded DNA with Single Base Resolution

Zhe He,[†] Zehua Han,[†] Megan Kizer,[‡] Robert J. Linhardt,[‡] Xing Wang,*[,‡] Alexander M. Sinyukov,[†] Jizhou Wang,[†] Volker Deckert,[§,∥] Alexei V. Sokolov,*[,†,⊥] Jonathan Hu,*[,⊥] and Marlan O. Scully*[,†,⊥]

[†]Texas A&M University, College Station, Texas 77843, United States
[‡]Rensselaer Polytechnic Institute, Troy, New York 12180, United States
[§]Friedrich-Schiller-Universitaet Jena, Lessingstraße 10, 07743 Jena, Germany
[∥]Leibniz Institute of Photonic Technology, Albert-Einsteinstraße 9, 07745 Jena, Germany
[⊥]Baylor University, Waco, Texas 76798, United States

Supporting Information

ABSTRACT: Tip-enhanced Raman scattering (TERS) is a promising optical and analytical technique for chemical imaging and sensing at single molecule resolution. In particular, TERS signals generated by a gap-mode configuration where a silver tip is coupled with a gold substrate can resolve a single-stranded DNA (ssDNA) molecule with a spatial resolution below 1 nm. To demonstrate the proof of subnanometer resolution, we show direct nucleic acid sequencing using TERS of a phage ssDNA (M13mp18). M13mp18 provides a known sequence and, through our deposition strategy, can be stretched (uncoiled) and attached to the substrate by its phosphate groups, while exposing its nucleobases to the tip. After deposition, we scan the silver tip along the ssDNA and collect TERS signals with a step of 0.5 nm, comparable to the bond length between two adjacent DNA bases. By demonstrating the real-time profiling of a ssDNA configuration and furthermore, with unique TERS signals of monomeric units of other biopolymers, we anticipate that this technique can be extended to the high-resolution imaging of various nanostructures as well as the direct sequencing of other important biopolymers including RNA, polysaccharides, and polypeptides.

Tip-enhanced Raman scattering (TERS) provides an effective technique at the forefront of the chemical imaging.[1] TERS can effectively enhance Raman signals by localized plasmon resonance on a nanoscale tip, increasing Raman signals by a factor of 10^6.[2,3] In addition, the near-field effects caused by nanoscale tips overcome the optical diffraction limit to allow high-resolution imaging of target molecules. Previous studies illustrated that TERS enables a resolution of near or less than 1 nm under ambient and cryogenic conditions for both STM and AFM based systems,[4−9] which may be due to the localization effects of atomic-scale structures on tips.[10,11] Furthermore, the gap-mode configuration generated in the plasmonic cavity formed between the silver tip and the gold substrate can further boost the enhancement factor of TERS to 10^{13}-fold within the gap.[12] These advantages make TERS an ideal technique for chemical identifications of single molecules.

Deoxyribonucleic acid (DNA) is an essential and information-rich biological molecule carrying the genetic information on all living organisms. The DNA molecule contains a linear sequence encoded by four nucleobases with prominently different Raman signals which provide a powerful tool for the determination of DNA nucleobase sequences.[13,14] To date, heroic progress has been made in single molecule sequencing (SMS). Among this progress, a nanopore-based sequencing method, a representative of the third-generation sequencing methods that focus on single molecule sequencing (SMS), is limited by the incredibly short dwell times of DNA in the nanopore and the poor resolution of the individual nucleobase signals,[15,16] resulting in sequencing errors. As a technology of high-resolution imaging, TERS provides an alternative application to analyze nucleobases without requiring the amplification of nucleic acids or labeled reagents and is not limited by the same factors that limit nanopore technology. So far, TERS has been demonstrated capable of distinguishing nucleobases[13,17] as well as enabling the exploration of DNA sensing,[18,19] hydrogen bonds[20] and aggregation effects.[21] For pure nucleic acids, a spatial resolution of 0.9 nm was obtained by using TERS to scan across the boundary of pure nucleobase networks.[17] A practical solution for reading nucleotides sequences along DNA bundles requires DNA with very simple sequences and careful scans along a DNA strand.[1]

Although TERS can distinguish individual nucleobases, imaging the single ssDNA molecule remains very challenging since stable alignment of the single DNA molecule is difficult and required to read nonoverlapping nucleotides. As further elaborated below, in this report for the first time we have demonstrated the success of single ssDNA imaging and using TERS to directly sequence multiple segments of the known M13mp18 bacteria phage ssDNA with at least 90% accuracy. Our success relies on (1) TERS imaging that leads to mapping DNA molecules and identifying sequences with a single-base resolution and (2) a unique DNA deposition method we have

Received: October 25, 2018
Published: December 26, 2018

DOI: 10.1021/jacs.8b11506
J. Am. Chem. Soc. 2019, 141, 753−757

developed for effectively minimizing DNA coiling as well as maximizing the exposure of nucleobases to the AFM tips (Figure 1).

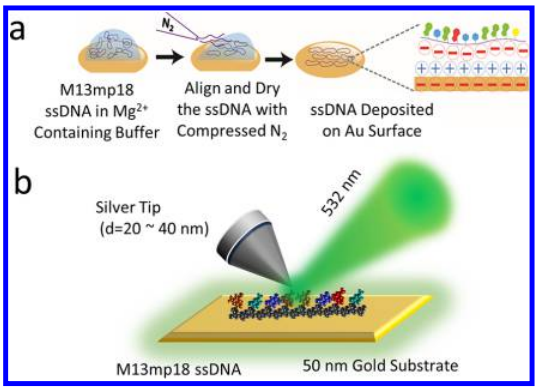

Figure 1. (a) The DNA deposition method. We used forced-air to align the ssDNA on the gold surface to stretch the DNA for evading/minimizing DNA coiling during the deposition. Furthermore, we added Mg^{2+} cations in the DNA buffer solution (pH 7.5) during the deposition to preferentially facilitate the adhesion of highly negatively charged DNA phosphate backbone to negatively charged gold surface. This will help to maximize the exposure of nucleobases to AFM tips for the downstream sensing and sequencing. Each '+' sign indicates a Mg^{2+} ion, and '−' sign indicates the negative charge carried by DNA phosphate backbone or the gold surface. (b) Schematic for tip-enhanced Raman scattering of ssDNA molecules. The diameter of the silver tip is 20 to 40 nm. An objective (100×, NA 0.7) focuses the 532 nm incidence light on the tip at 45°. TERS signals are collected by the same objective. Gap-mode TERS is formed by reducing tip−substrate distances to less than 1 nm.

We show a tapping-mode AFM image in Figure 2 and estimate the thickness of a ssDNA strand at approximately 0.6 nm. Because the thickness of the M13mp18 ssDNA was reported to be 0.3 ± 0.1 nm,[22] it is reasonable to assume that this represents a planar bundle of one to two nucleobase height. However, it is noted that AFM cannot precisely measure the width of a ssDNA molecule because its lateral resolution is limited by the tip broadening effects.

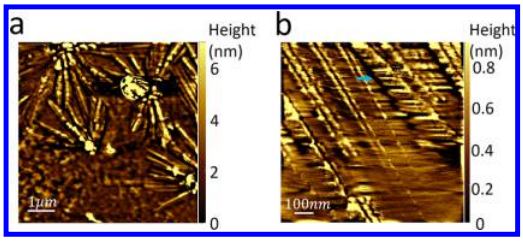

Figure 2. DNA sensing by AFM. (a) AFM image of DNA clusters and (b) a zoom-in image of the red dash-line squared region in panel a.

Compared to AFM, TERS provides a superior, subnanometer resolution of the bundle edges. We performed a TERS scan along the blue arrow as indicated in Figure 2b with a step size of 0.5 nm. We set the acquisition time as 4 s to attenuate the effects of spectral fluctuations for achieving stable measurements. Shown by the red curve in Figure 3a, the integrated intensities of the Raman signal peaks from 1630 to 1650 cm^{-1} can refer to DNA nucleobases cytosine (C), guanine (G) and thymine (T). The width of the DNA bundle

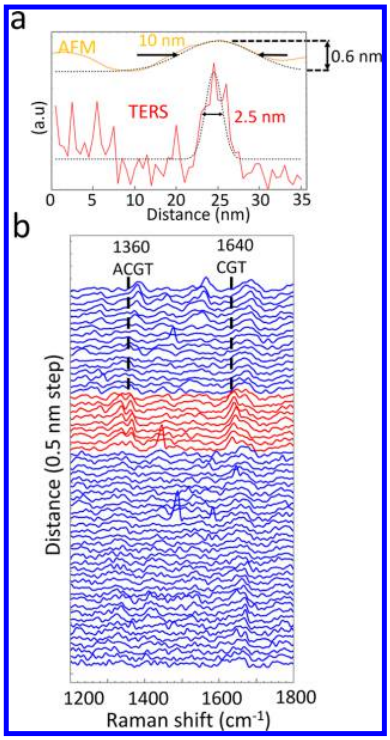

Figure 3. (a) AFM (yellow) and TERS (red) signals collected along the blue arrow in panel b. We use AFM and TERS to estimate the width of a DNA bundle. The AFM curve exhibits a full-width at half-maximum (fwhm) of 10 nm based on a Gaussian fitting. The TERS curve, which is the integrated intensity of the Raman signal from 1630 to 1650 cm^{-1}, exhibits a fwhm of 2.5 nm, far narrower than AFM. (b) TERS spectra taken along the blue arrow in Figure 2b. The scanning step is 0.5 nm. The red curves represent the spectra on the DNA bundle.

is estimated to be 2.5 nm. Similarly, in Figure 4a, we imaged the sample based on the same peaks. The high contrast map highlights a single DNA strand (spot 1 to 24). Moreover, the one-step spectral changes from the red to blue parts in Figure 3b and the distinguishable on-strand and off-strand signals in Figure 4b prove that TERS was able to reach a spatial resolution of 0.5 nm.

In this study, we chose the scanning step of 0.5 nm to be comparable to the base-to-base distance, which was reported as 0.4 to 0.6 nm.[23−25] A choice of step size larger than 0.6 nm would be inadequate for sequence mapping. In contrast, a step size smaller than 0.4 nm can lead to difficulties in distinguishing homogeneous sequences such as "AAAAA" from "AAAA". Moreover, when the step size is comparable to the base interval, the tip apex could possibly "push" nucleobases and rearrange these at each step. Although the distances between bases are initially varied due to the random rotation of nucleotides, the tip may shift them to a certain degree, so that these distances become approximately equal to the step size of TERS scanning, which may lead to the capability of detecting one base in one step. Moreover, DNA strands were possibly pushed by the tip apex and showed themselves as a line along the horizontal direction. It has been reported that the AFM tip, operating in the contact mode, can move carbon nanotubes.[26] In our case, although the AFM was operated in the tapping mode, the TERS scanning could

DOI: 10.1021/jacs.8b11506
J. Am. Chem. Soc. 2019, 141, 753−757

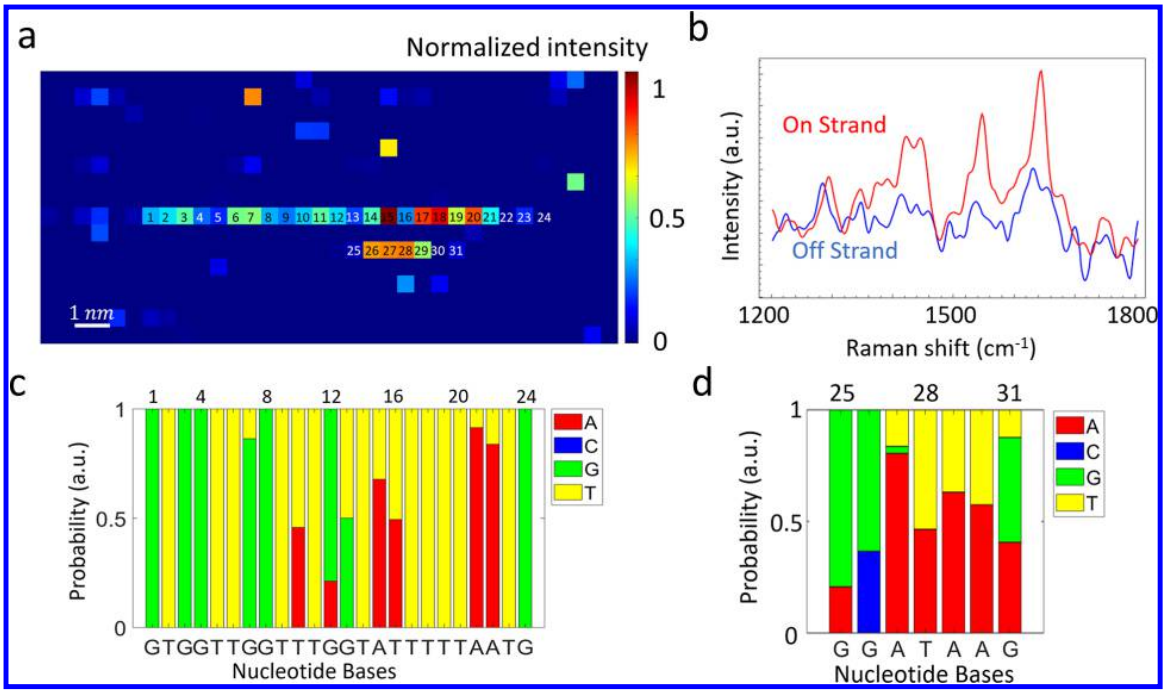

Figure 4. DNA sequencing of sample 1 containing 1.0 pmol of M13mp18 DNA. (a) TERS image of a single ssDNA segment with a step size of 0.5 nm. The acquisition time for each step is 4 s. The plots show the integral intensities of the spectrum from 1630 to 1650 cm^{-1}. The numbers marking the map indicate the order of the sequences. (b) The "on strand" TERS spectrum of the pixel 7 and the "off strand" spectrum one step above the pixel 7 in panel a. The substantial difference proves the 0.5 nm resolving capacity along the cross section. (c) A bar chart shows the probabilities P_i from the spot 1 to 24 labeled in panel a. The most probable bases are labeled at the bottom. Compared to the real DNA sequence GTGGTTCGTTCGGTATTTTTAATG, two errors are found at the spot 7 (G→ C) and spot 11 (T → C). (d) The probabilities P_i from the spot 25 to 31. Two strands in panel a are 1 nm separated. The different sequences of spots 13 to 19 and spots 25 to 31 provides an evidence that TERS imaging can distinguish two parallel DNA molecules only separated by 1 nm.

resemble a contact procedure and realign the strands. Meanwhile, because the vibration frequency of the cantilever is close to the oscillation resonance, the tip will still perform strong tapping force toward the ssDNA molecules.[27] The lateral pressure may also cause the ssDNA realignment.

We then identify the characteristic peaks of each nucleobase used to identify the nucleobases sequences. Summarized in Table S1, Raman peaks at 735 to 737 cm^{-1} (A1), 1467 to 1492 cm^{-1} (A2), 799 to 801 cm^{-1} (C1), 1235 to 1270 cm^{-1} (C2), 954 to 958 cm^{-1} (G1), 1545 to 1554 cm^{-1} (G2), and 778 to 782 cm^{-1} (T1), 1366 to 1373 cm^{-1} (T2) are utilized to distinguish adenine (A), cytosine (C), guanine (G) and thymine (T).[1,13,28−31] Four spectral references were then built according to the modes A1, A2, C1, C2, G1, G2, T1 and T2 (Figure S3). Moreover, Figure S4 and Figure S5 display these identifiable modes in our measurement. Baseline correction by a third order polynomial fitting was applied to TERS spectra. The linear correlation between the scanning spectra and the templates was based on the discrete Pearson correlation function.[32] The normalized correlation coefficient can be found to evaluate probabilities P_i of four nucleobases. As described below, repeating the calculations (see Supporting Information) for all spots, we determined the sequences of each scanned DNA segment. Then, by comparing these data with the actual sequence of M13mp18 DNA through approximate string matching,[33] we proved the credibility of our TERS sequencing results.

Identified DNA sequences are shown in Figure 4c,d. We used the same tip as in Figure 3. Because interferences of adjacent bases result in multicomponent signals, we label the most possible bases below the bar charts. The multicomponent spectrum occurs due to the interference of adjacent bases. Mistakes may happen when the surrounding signals overwhelm the target base. Therefore, in Figure 4c, spot 7 and spot 11 were misread due to the strong signals of guanine and thymine. The accuracy shown in Figure 4c is 91.7% (22/24). Six repeated measurements in Figure S1 and Table S2 show the sequencing accuracy, using different tips and different deposited samples, is better than 90.9%.

To prove that the measured sequences of each segment truly matched the actual M13mp18 sequence, we constructed a random 24-base trial sequence as a comparison and applied approximate string-matching algorithm for 10 million times. Under the best matching conditions between a 24-base random sequence and any 24-base long segment of M13mp18, the average number of mismatching errors was 9.4. The probability of 2 errors for a random trial is less than 1/10,000,000. The distribution of mismatching errors for trials using random sequences are shown in Figure S2. This negligible probability proves that our sequencing result is authentic, and the sequence from spot 1 to spot 24 belongs to a specific fragment of the M13mp18 DNA. The similar comparison was repeated for each repeating result in Table S2.

In conclusion, by displaying ssDNA imaging and sequencing at room temperature, we have demonstrated the subnanometer resolving ability of TERS and have shown the repeatability of using different tips and ssDNA molecules. As a straightforward optical sensing technique, TERS has the potential of becoming

DOI: 10.1021/jacs.8b11506
J. Am. Chem. Soc. 2019, 141, 753−757

a next generation sequencing method for DNA/RNA as well as other important biological polymers such as polysaccharides, polypeptides, and even glyco-peptide conjugates.

■ ASSOCIATED CONTENT

Supporting Information

The Supporting Information is available free of charge on the ACS Publications website at DOI: 10.1021/jacs.8b11506.

Sample preparation, measurements, data analysis, Raman peak assignments, repeating results, random sequence testing, spectral templates of nucleobases (PDF)

■ AUTHOR INFORMATION

Corresponding Authors

*wangx28@rpi.edu
*sokol@physics.tamu.edu
*jonathan_hu@baylor.edu
*scully@tamu.edu

ORCID

Zhe He: 0000-0002-8525-3650
Megan Kizer: 0000-0003-3549-8606
Robert J. Linhardt: 0000-0003-2219-5833
Xing Wang: 0000-0001-9930-3287
Volker Deckert: 0000-0002-0173-7974
Jonathan Hu: 0000-0001-6426-3051

Notes

The authors declare no competing financial interest.

■ ACKNOWLEDGMENTS

This work was supported by the Office of Naval Research (grants N00014-16-1-3054 and N00014-16-1-2578), the Robert A. Welch Foundation (awards A1261 and A-1547), Air Force Office of Scientific Research (Award No. FA9550-18-1-0141) and the National Science Foundation (grants CHE-1609608 and ECCS-1809622). X.W. thanks the support from the CBIS Facility Award and the gift fund from HT Materials Corporation. M.K. thanks the support from Slezak Memorial Fellowship Award and Maas Prize. J.H. thanks the support from the Baylor Young Investigator Development Award. Z.H. is supported by the Herman F. Heep and Minnie Belle Heep Texas A&M University Endowed Fund held/administered by the Texas A&M Foundation.

■ REFERENCES

(1) Lin, X.-M.; Deckert-Gaudig, T.; Singh, P.; Siegmann, M.; Kupfer, S.; Zhang, Z.; Gräfe, S.; Deckert, V. Direct Base-to-Base Transitions in ssDNA Revealed by Tip-Enhanced Raman Scattering. *arXiv:1604.06598* **2016**.

(2) Jiang, N.; Foley, E. T.; Klingsporn, J. M.; Sonntag, M. D.; Valley, N. A.; Dieringer, J. A.; Seideman, T.; Schatz, G. C.; Hersam, M. C.; Van Duyne, R. P. Observation of Multiple Vibrational Modes in Ultrahigh Vacuum Tip-Enhanced Raman Spectroscopy Combined with Molecular-Resolution Scanning Tunneling Microscopy. *Nano Lett.* **2012**, *12* (10), 5061−5067.

(3) Pettinger, B.; Ren, B.; Picardi, G.; Schuster, R.; Ertl, G. Nanoscale Probing of Adsorbed Species by Tip-Enhanced Raman Spectroscopy. *Phys. Rev. Lett.* **2004**, *92* (9), 096101.

(4) Chen, C.; Hayazawa, N.; Kawata, S. A 1.7 Nm Resolution Chemical Analysis of Carbon Nanotubes by Tip-Enhanced Raman Imaging in the Ambient. *Nat. Commun.* **2014**, *5*, 3312.

(5) Zhang, R.; Zhang, Y.; Dong, Z. C.; Jiang, S.; Zhang, C.; Chen, L. G.; Zhang, L.; Liao, Y.; Aizpurua, J.; Luo, Y.; et al. Chemical Mapping of a Single Molecule by Plasmon-Enhanced Raman Scattering. *Nature* **2013**, *498* (7452), 82−86.

(6) Deckert-Gaudig, T.; Kurouski, D.; Hedegaard, M. A. B.; Singh, P.; Lednev, I. K.; Deckert, V. Spatially Resolved Spectroscopic Differentiation of Hydrophilic and Hydrophobic Domains on Individual Insulin Amyloid Fibrils. *Sci. Rep.* **2016**, *6*, 33575.

(7) Jiang, S.; Zhang, Y.; Zhang, R.; Hu, C.; Liao, M.; Luo, Y.; Yang, J.; Dong, Z.; Hou, J. G. Distinguishing Adjacent Molecules on a Surface Using Plasmon-Enhanced Raman Scattering. *Nat. Nanotechnol.* **2015**, *10* (10), 865−869.

(8) Kurouski, D.; Deckert-Gaudig, T.; Deckert, V.; Lednev, I. K. Structure and Composition of Insulin Fibril Surfaces Probed by TERS. *J. Am. Chem. Soc.* **2012**, *134* (32), 13323−13329.

(9) Richard-Lacroix, M.; Zhang, Y.; Dong, Z.; Deckert, V. Mastering High Resolution Tip-Enhanced Raman Spectroscopy: Towards a Shift of Perception. *Chem. Soc. Rev.* **2017**, *46* (13), 3922−3944.

(10) Trautmann, S.; Aizpurua, J.; Götz, I.; Undisz, A.; Dellith, J.; Schneidewind, H.; Rettenmayr, M.; Deckert, V. A Classical Description of Subnanometer Resolution by Atomic Features in Metallic Structures. *Nanoscale* **2017**, *9* (1), 391−401.

(11) Urbieta, M.; Barbry, M.; Zhang, Y.; Koval, P.; Sánchez-Portal, D.; Zabala, N.; Aizpurua, J. Atomic-Scale Lightning Rod Effect in Plasmonic Picocavities: A Classical View to a Quantum Effect. *ACS Nano* **2018**, *12* (1), 585−595.

(12) Marr, J. M.; Schultz, Z. D. Imaging Electric Fields in SERS and TERS Using the Vibrational Stark Effect. *J. Phys. Chem. Lett.* **2013**, *4* (19), 3268.

(13) Treffer, R.; Lin, X.; Bailo, E.; Deckert-Gaudig, T.; Deckert, V. Distinction of Nucleobases − a Tip-Enhanced Raman Approach. *Beilstein J. Nanotechnol.* **2011**, *2* (1), 628−637.

(14) Cao, Y. C.; Jin, R.; Mirkin, C. A. Nanoparticles with Raman Spectroscopic Fingerprints for DNA and RNA Detection. *Science* **2002**, *297* (5586), 1536−1540.

(15) Heather, J. M.; Chain, B. The Sequence of Sequencers: The History of Sequencing DNA. *Genomics* **2016**, *107* (1), 1−8.

(16) Agah, S.; Zheng, M.; Pasquali, M.; Kolomeisky, A. B. DNA Sequencing by Nanopores: Advances and Challenges. *J. Phys. D: Appl. Phys.* **2016**, *49* (41), 413001.

(17) Zhang, R.; Zhang, X.; Wang, H.; Zhang, Y.; Jiang, S.; Hu, C.; Zhang, Y.; Luo, Y.; Dong, Z. Distinguishing Individual DNA Bases in a Network by Non-Resonant Tip-Enhanced Raman Scattering. *Angew. Chem., Int. Ed.* **2017**, *56* (20), 5561−5564.

(18) Bailo, E.; Deckert, V. Tip-Enhanced Raman Spectroscopy of Single RNA Strands: Towards a Novel Direct-Sequencing Method. *Angew. Chem., Int. Ed.* **2008**, *47* (9), 1658−1661.

(19) Najjar, S.; Talaga, D.; Schué, L.; Coffinier, Y.; Szunerits, S.; Boukherroub, R.; Servant, L.; Rodriguez, V.; Bonhommeau, S. Tip-Enhanced Raman Spectroscopy of Combed Double-Stranded DNA Bundles. *J. Phys. Chem. C* **2014**, *118* (2), 1174−1181.

(20) Zhang, D.; Domke, K. F.; Pettinger, B. Tip-Enhanced Raman Spectroscopic Studies of the Hydrogen Bonding between Adenine and Thymine Adsorbed on Au (111). *ChemPhysChem* **2010**, *11* (8), 1662−1665.

(21) Pashaee, F.; Tabatabaei, M.; Caetano, F. A.; Ferguson, S. G.; Lagugné-Labarthet, F. Tip-Enhanced Raman Spectroscopy: Plasmid-Free vs. Plasmid-Embedded DNA. *Analyst* **2016**, *141* (11), 3251−3258.

(22) Adamcik, J.; Klinov, D. V.; Witz, G.; Sekatskii, S. K.; Dietler, G. Observation of Single-Stranded DNA on Mica and Highly Oriented Pyrolytic Graphite by Atomic Force Microscopy. *FEBS Lett.* **2006**, *580* (24), 5671−5675.

(23) Grange, W.; Duckely, M.; Husale, S.; Jacob, S.; Engel, A.; Hegner, M. VirE2: A Unique SsDNA-Compacting Molecular Machine. *PLoS Biol.* **2008**, *6* (2), e44.

(24) Chen, W.-s.; Chen, W.-H.; Chen, Z.; Gooding, A. A.; Lin, K.-J.; Kiang, C.-H. Direct Observation of Multiple Pathways of Single-Stranded DNA Stretching. *Phys. Rev. Lett.* **2010**, *105* (21) DOI: 10.1103/PhysRevLett.105.218104.

(25) Candelli, A.; Modesti, M.; Peterman, E. J. G.; Wuite, G. J. L. Single-Molecule Views on Homologous Recombination. *Q. Rev. Biophys.* **2013**, *46* (4), 323−348.
(26) Yano, T.; Ichimura, T.; Kuwahara, S.; H'Dhili, F.; Uetsuki, K.; Okuno, Y.; Verma, P.; Kawata, S. Tip-Enhanced Nano-Raman Analytical Imaging of Locally Induced Strain Distribution in Carbon Nanotubes. *Nat. Commun.* **2013**, *4*, 2592.
(27) Li, M.; Dang, D.; Liu, L.; Xi, N.; Wang, Y. Imaging and Force Recognition of Single Molecular Behaviors Using Atomic Force Microscopy. *Sensors* **2017**, *17* (1), 200.
(28) Madzharova, F.; Heiner, Z.; Gühlke, M.; Kneipp, J. Surface-Enhanced Hyper-Raman Spectra of Adenine, Guanine, Cytosine, Thymine, and Uracil. *J. Phys. Chem. C* **2016**, *120* (28), 15415−15423.
(29) Yang, S. Y.; Butler, I. S. Pressure-Tuning Infrared and Raman Microscopy Study of the DNA Bases: Adenine, Guanine, Cytosine, and Thymine. *J. Biomol. Struct. Dyn.* **2013**, *31* (12), 1490−1496.
(30) Peticolas, W. L. [17] Raman Spectroscopy of DNA and Proteins. In *Methods in Enzymology; Biochemical Spectroscopy*; Academic Press, 1995; Vol. *246*, pp 389−416.
(31) De Gelder, J.; De Gussem, K.; Vandenabeele, P.; Moens, L. Reference Database of Raman Spectra of Biological Molecules. *J. Raman Spectrosc.* **2007**, *38* (9), 1133.
(32) Griffiths, P. R.; Shao, L. Self-Weighted Correlation Coefficients and Their Application to Measure Spectral Similarity. *Appl. Spectrosc.* **2009**, *63* (8), 916−919.
(33) Kawulok, J. Approximate String Matching for Searching DNA Sequences. *Int. J. Biosci., Biochem. Bioinf.* **2013**, 145−148.

DOI: 10.1021/jacs.8b11506
J. Am. Chem. Soc. 2019, 141, 753−757